Journal of Quantitative Spectroscopy & Radiative Transfer 112 (2011) 1257–1265

Contents lists available at ScienceDirect

Journal of Quantitative Spectroscopy & Radiative Transfer

journal homepage: www.elsevier.com/locate/jqsrt

The $a^1\Delta_g$–$X^3\Sigma_g^-$ band of $^{16}O^{17}O$, $^{17}O^{18}O$ and $^{17}O_2$ by high sensitivity CRDS near 1.27 μm

Olga Leshchishina [a,b], Samir Kassi [a], Iouli E. Gordon [c], Shanshan Yu [d], Alain Campargue [a,*]

[a] Université Grenoble 1/CNRS, UMR5588 LIPHY, Grenoble, F-38041, France
[b] Laboratory of Theoretical Spectroscopy, Zuev Institute of Atmospheric Optics, 1 Akademicheskii av., 634021 Tomsk, Russia
[c] Harvard-Smithsonian Center for Astrophysics, Atomic and Molecular Physics Division, Cambridge, MA 02138, USA
[d] Jet Propulsion Laboratory, California Institute of Technology, Pasadena, CA 91109-8099, USA

ARTICLE INFO

Article history:
Received 21 December 2010
Accepted 16 January 2011
Available online 20 January 2011

Keywords:
Oxygen
O_2
^{17}O isotopologues
Hyperfine structure
Cavity ring down spectroscopy
Cryogenic cell

ABSTRACT

The very weak $a^1\Delta_g$–$X^3\Sigma_g^-$ system of the three ^{17}O isotopologues of oxygen – $^{16}O^{17}O$, $^{17}O^{18}O$ and $^{17}O_2$ – was studied by high sensitivity CW-Cavity Ring Down Spectroscopy. The spectra of a ^{17}O highly enriched sample were recorded at room temperature between 7640 and 7917 cm^{-1} and at liquid nitrogen temperature in the 7876–7893 cm^{-1} region. The magnetic dipole (0–0) band was observed for all three ^{17}O isotopologues. At liquid nitrogen temperature, some of the transitions were observed with partially resolved hyperfine splitting due to the ^{17}O nuclear spin. The electric quadrupole (0–0) band and the (1–1) hot band were also observed for the $^{16}O^{17}O$ and $^{17}O_2$ species. The rotational and hyperfine spectroscopic parameters of the $X^3\Sigma_g^-$ and $a^1\Delta_g$ states of the three studied isotopologues were derived from a global fit of the measured line positions and microwave and Raman measurements available in the literature. The spectroscopic constants of the $a^1\Delta_g$ (v=0, 1) states of $^{17}O_2$ are reported for the first time.

1. Introduction

We have recently applied the Cavity Ring Down Spectroscopy (CRDS) technique to investigate the $a^1\Delta_g$–$X^3\Sigma_g^-$ band of oxygen [1,2]. These studies were initially motivated by the detection of electric quadrupole transitions in the atmospheric solar spectrum showing the necessity of improving the spectral parameters of the $a^1\Delta_g$–$X^3\Sigma_g^-$ band of molecular oxygen from new laboratory measurements [1]. The high sensitivity CRDS spectra of "natural" and ^{18}O-enriched oxygen revealed not only the electric quadrupole transitions but also the magnetic dipole (1–1) hot bands of $^{16}O_2$ and $^{18}O_2$, and allowed detecting new rotational transitions of the (0–0) band of the five most abundant oxygen isotopologues ($^{16}O_2$, $^{16}O^{18}O$, $^{18}O_2$, $^{16}O^{17}O$ and $^{17}O^{18}O$) [1,2]. These measurements combined with microwave (MW) and Raman data available in the literature allowed deriving the best to date spectroscopic constants for the $X^3\Sigma_g^-$ and $a^1\Delta_g$ states [2].

In the present work, we extended the observations for the ^{17}O-containing isotopologues from CRDS spectra recorded with a sample highly enriched in ^{17}O. As a consequence of the non-zero nuclear spin of the ^{17}O nucleus (I=5/2), low rotational transitions show a hyperfine (hf) splitting. Indeed in the room temperature spectra reported in Ref. [2], the line profiles of some transitions of $^{16}O^{17}O$ and $^{17}O^{18}O$ were observed to be broadened due to an unresolved hyperfine structure. We have recently shown that the combination of the high sensitivity CRDS technique with a cryogenic cell at 80 K allows for a significantly better

* Corresponding author. Tel.: +33 4 76 51 43 19; fax: +33 4 76 63 54 95.
E-mail address: Alain.CAMPARGUE@ujf-grenoble.fr (A. Campargue).

0022-4073/$ - see front matter © 2011 Elsevier Ltd. All rights reserved.
doi:10.1016/j.jqsrt.2011.01.014

resolution of the hyperfine structure of the ^{17}O-containing isotopologues [3].

The present contribution consists in the full analysis of the spectra and the derivation of the spectroscopic parameters from a global fit of the line positions combined with microwave and Raman data available in the literature [4–6]. Note that apart from our CRDS observations of the $a^1\Delta_g$ state through the $a^1\Delta_g$–$X^3\Sigma_g^-$ band [1,2], the only previous high resolution study of the $a^1\Delta_g$ electronic state in $^{16}O^{17}O$ and $^{17}O^{18}O$ was reported from electron paramagnetic resonance (EPR) spectra of the J=2 level [7]. To the best of our knowledge, no spectroscopic data relative to the $a^1\Delta_g$ state of $^{17}O_2$ are available in the literature.

2. Experimental details and sample composition

The high sensitivity CW-CRDS absorption spectrum of the $a^1\Delta_g$–$X^3\Sigma_g^-$ band of oxygen was recorded at room temperature (RT) in the 7658–7917 cm^{-1} region, using a highly enriched in ^{17}O sample. The stated atomic composition of the sample (from Sigma Aldrich) was ^{17}O: 55.8%, ^{16}O: 43.4% and ^{18}O: 0.8%. The pressure value of the recordings was fixed to 30.0 Torr and the room temperature value was 296 K. Additional recordings at 5.0 Torr were performed in the 7839–7917 cm^{-1} region in order to avoid saturation of the strongest lines. The overview of the $a^1\Delta_g$–$X^3\Sigma_g^-$ band is presented in Fig. 1.

The fibered distributed feedback (DFB) laser CW-CRDS spectrometer used for the recordings is the same as the one used for the study of the natural and ^{18}O-enriched samples [1,2]. The experimental setup has been described in detail in Refs. [8–10]. Each DFB laser diode has a typical tuning range of about 40 cm^{-1} by temperature tuning from −10 to 60 °C. A total of nine DFB laser diodes were required to cover the 7658–7917 cm^{-1} region. The electro-polished stainless steel ring down cell (l=1.42 m, inner diameter Φ=11 mm) was fitted by a pair of supermirrors. The reflectivity of these mirrors (about 99.997%) corresponds to empty cell ring down times of about $\tau\sim$200 μs. About 40 ring down events were averaged for each spectral data point; the complete temperature scan of one DFB laser required about 70 min. The achieved noise equivalent absorption was about $\alpha_{min}\sim 4\times 10^{-11}$ cm^{-1} over the whole spectrum. The pressure measured by a capacitance gauge (MKS 100 Torr full range with 0.1% accuracy) and the ring down cell temperature were monitored during the recordings.

Due to the Doppler broadening, the hf structure cannot be fully resolved at room temperature and shows up only as an additional broadening of the transitions of the ^{17}O-containing isotopologues [2]. In order to decrease the Doppler broadening by a factor of 2, the spectrum in the 7876–7893 cm^{-1} region was also recorded at 80 ± 2 K, hereafter referred as liquid nitrogen temperature (LNT) [3]. This spectral section corresponds to the low rotational transitions, which exhibit the largest hyperfine splittings. The cryogenic cell has been described in Refs. [11–14]. It was developed and extensively used to characterize the absorption spectrum of methane at low temperature in the 1.58 and 1.28 μm methane transparency windows [11–14]. The pressure value of the LNT recordings was fixed to 1.5 Torr. The comparison between the 296 and 80 K spectra (Fig. 2) illustrates the gain in the resolution of the hf structure resulting from the reduction of the Doppler broadening.

Each 40 cm^{-1} wide spectrum recorded with one DFB laser was calibrated independently on the basis of the wavelength values provided by a Michelson-type wavemeter (Bristol 621A, 60 MHz resolution and 100 MHz absolute accuracy). The calibration was further refined by stretching the whole spectrum in order to match accurate positions of the transitions of the $a^1\Delta_g$–$X^3\Sigma_g^-$ band of $^{16}O_2$ provided in the recent HITRAN update [15]. The typical uncertainty in the line positions is estimated to be less than 1×10^{-3} cm^{-1}.

The determination of the line centers and line intensities was difficult because of the superposition of many hf components, which are only partly resolved. The line profile analysis was adapted according to the impact of the hf structure on the observed line profile:

(i) A detailed analysis of the hf structure was performed only for the few first rotational transitions recorded at LNT because these transitions show the most resolved hf structure. Eight, six and four hf manifolds

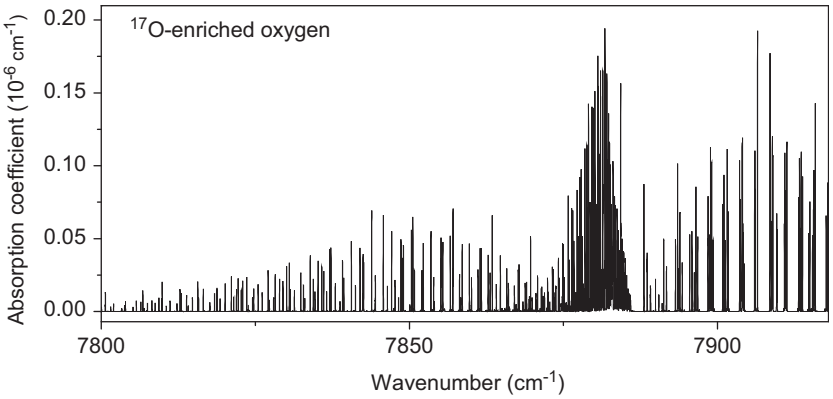

Fig. 1. Overview of the $a^1\Delta_g$–$X^3\Sigma_g^-$ system of oxygen recorded by CW-CRDS (P=30.0 Torr, T=296 K) with a highly ^{17}O-enriched sample. The relative abundances in the sample were the following: $^{16}O^{17}O$: 0.469, $^{17}O_2$: 0.330, $^{16}O_2$: 0.184, $^{17}O^{18}O$: 9.6×10^{-3} and $^{16}O^{18}O$: 7.02×10^{-3}.

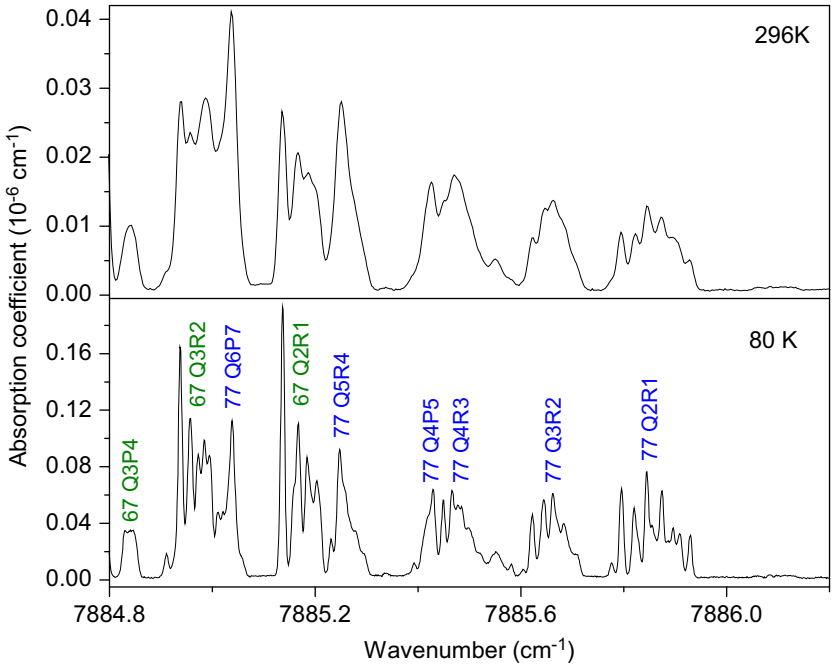

Fig. 2. Partly resolved hyperfine structure of $^{16}O^{17}O$ and $^{17}O_2$ transitions at 296 and 80 K in the region of the QR and QP branches. The spectra recorded at 296 K (P=5.0 Torr) and 80 K (P=1.5 Torr) are shown on the upper and lower panel, respectively.

Table 1
Summary of the CW-CRDS observations for the $a^1\Delta_g$–$X^3\Sigma_g^-$ band system of ^{17}O highly enriched oxygen near 1.27 μm.

Isotopologue	HITRAN notation	Relative abundance	Band	Number of lines	Intensity range[a] ($\times 10^{-26}$ cm/molecule)
$^{16}O^{17}O$	67	0.469(30)	(0–0)	206	3.79×10^{-4}–3.55
			(0–0) elec. quad.	12	3.77×10^{-4}–4.93×10^{-3}
			(1–1)	68	1.35×10^{-4}–1.71×10^{-3}
$^{17}O_2$	77	0.330(30)	(0–0)	209	2.04×10^{-4}–2.96
			(0–0) elec. quad.	8	2.66×10^{-4}–6.82×10^{-4}
			(1–1)	39	1.36×10^{-4}–1.61×10^{-3}
$^{16}O_2$	66	0.184(7)	(0–0)	89	2.95×10^{-4}–1.89
			(0–0) elec. quad.	5	3.93×10^{-4}–5.02×10^{-4}
			(1–1)	24	2.75×10^{-4}–7.84×10^{-4}
$^{17}O^{18}O$	78	$9.6(18)\times10^{-3}$	(0–0)	105	3.5×10^{-4}–4.7×10^{-2}
$^{16}O^{18}O$	68	$7.02(92)\times10^{-3}$	(0–0)	78	2.53×10^{-4}–3.86×10^{-2}

[a] The given intensity values include the relative abundance in the sample.

were considered for $^{16}O^{17}O$, $^{17}O_2$ and $^{17}O^{18}O$, respectively. The line centers and intensities were determined using an interactive least squares multi-line fitting program assuming a Voigt profile (http://sourceforge.net/projects/fityk/ version v 0.8.6). The integrated absorption coefficient, position, Gaussian and Lorentzian widths of each line and the corresponding local baseline (assumed to be a linear function of the wavenumber) were obtained from the multi-line fit.

(ii) In the case of the high rotational transitions of the RT spectrum, showing negligible hf structure, the transitions were considered as single lines and the same program was used to fit the line profile.

(iii) The most challenging situation is the intermediate case where the lines show a wide, generally asymmetric and mostly unresolved profile due to the hf structure. To minimize the negative effect of the unresolved hf structure, the line centers were determined as an average value over the line profile of the wavenumbers weighted by the corresponding absorption coefficient, the line intensities being obtained from the integrated absorption coefficient.

More details about the combination of the RT and LNT experimental data for the fit of the spectroscopic parameters are given in Section 5.

Overall more than one thousand lines due to the $^{17}O_2$, $^{16}O^{17}O$, $^{16}O^{18}O$, $^{17}O^{18}O$ and $^{16}O_2$ were measured in the room temperature spectrum. Some lines due to impurities (mostly H_2O but also N_2O, CO_2 and HF) were also identified.

On the basis of the HITRAN intensity values [15], the relative abundances of the $^{16}O^{18}O$ and $^{16}O_2$ species were calculated to be $7.02(92)\times10^{-3}$ and 0.184(7), respectively. In order to estimate the relative concentration of $^{16}O^{17}O$ and $^{17}O^{18}O$, we assumed the same band strength as for the $^{16}O^{18}O$ species, leading to the values of 0.469(30) and $9.6(18)\times10^{-3}$ for $^{16}O^{17}O$ and $^{17}O^{18}O$, respectively. From these estimated molecular concentrations we derived the following atomic composition: ^{17}O: 56.9%, ^{16}O: 42.2%, ^{18}O: 0.83%, which is in very good agreement with the stated atomic composition (^{17}O: 55.8%, ^{16}O: 43.4%, ^{18}O: 0.8%). Note that the concentration of impurities was negligible: H_2O and CO_2 concentrations were calculated to be less than 1.5×10^{-4} and 10^{-4}, respectively. Table 1 summarizes the observations and sample composition and provides the number of lines assigned to the different bands together with their intensity range.

3. Spectrum assignment

Only magnetic dipole and electric quadrupole transitions are possible in the $a^1\Delta_g$–$X^3\Sigma_g^-$ system of oxygen molecule. The $X^3\Sigma_g^-$ ground state obeys Hund's case (b_J) coupling: each $N>1$ rotational level splits into three components with **J=N+S** ($J=N+1$, N, $N-1$), where **J** is the total angular momentum, **N** is the rotational angular momentum and **S** is the total electron spin. These components are further split into hyperfine components **F=J+I**, with $F=J+I$, $J+I-1$, $\ldots|J-I|$. The $a^1\Delta_g$ upper state has zero total electron spin and therefore $J=N$.

The magnetic dipole transitions of the $a^1\Delta_g$–$X^3\Sigma_g^-$ system follow the $\Delta J=\pm1$, 0 selection rule leading to the observation of nine branches that we label here as $\Delta N(N'')\Delta J(J'')$.

In the first stage of the analysis, the assignments of the $^{16}O^{17}O$ and $^{17}O^{18}O$ transitions were transferred from our previous work [2]. The first assignments of the $a^1\Delta_g$–$X^3\Sigma_g^-$ (0–0) band of $^{17}O_2$ were performed from a rough simulation based on the $^{16}O^{18}O$ band with the frequency axis shifted and scaled according to the ratio of the B rotational constants [5]. The assignments of all the bands were then iteratively extended during the fit of the spectroscopic parameters.

Recently the electric quadrupole transitions in the $a^1\Delta_g$–$X^3\Sigma_g^-$ band of $^{16}O_2$ and $^{18}O_2$ were detected [1,2]. Their positions can be accurately predicted using spectroscopic constants obtained from magnetic dipole transitions [1]. The electric quadrupole transitions follow the $\Delta J=\pm2$, ±1, 0 selection rule, leading to 15 possible branches, but the $\Delta J=\pm1$ and 0 transitions coincide with much stronger magnetic dipole transitions and are not observable. In the present work, eight and twelve electric quadrupole transitions could be detected for $^{17}O_2$ and $^{16}O^{17}O$, respectively.

The achieved experimental sensitivity allowed the first detection of the $a^1\Delta_g$–$X^3\Sigma_g^-$ (1–1) hot band of $^{16}O^{17}O$ and $^{17}O_2$ which has a relative intensity of about 6×10^{-4} compared to the (0–0) band. The first assignments of the hot bands were performed on the basis of predictions obtained using the predicted rovibrational constants. The vibrational frequency, the B and D rotational constants in the $a^1\Delta_g$ and $X^3\Sigma_g^-$ states were predicted using the $^{16}O_2$ corresponding values and the usual mass dependence expression of the considered parameters [16]. The assignments of these weak transitions were made possible by the good accuracy of these predicted spectra: the

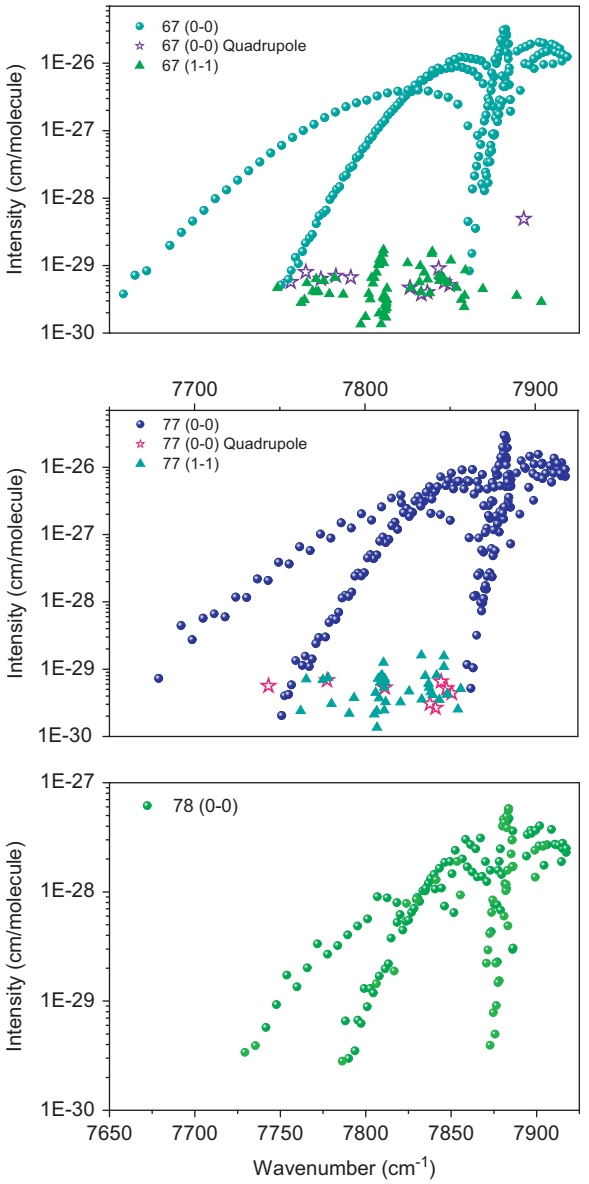

Fig. 3. Overview of the line lists of $^{16}O^{17}O$ (upper panel) and $^{17}O_2$ (middle panel) and $^{17}O^{18}O$ (lower panel). Full circles, full triangles and open stars correspond to the $a^1\Delta_g$–$X^3\Sigma_g^-$ (0–0) band, (1–1) hot band and electric quadrupole transitions, respectively. The $^{17}O^{18}O$ data set was completed with some lines measured in Ref. [2], when these lines were obscured by much stronger transitions in the present recordings. The intensity values include the relative abundances: 0.469, 0.330 and 9.6×10^{-3} for $^{16}O^{17}O$, $^{17}O_2$ and $^{17}O^{18}O$, respectively.

maximum deviations between predicted and measured line positions are on the order of 30×10^{-3} cm^{-1}. Finally we were able to assign the 39 and 68 transitions of the very weak $a^1\Delta_g$–$X^3\Sigma_g^-$ (1–1) hot band of $^{17}O_2$ and $^{16}O^{17}O$, respectively.

The overview of the $a^1\Delta_g$–$X^3\Sigma_g^-$ transitions assigned to $^{17}O_2$, $^{16}O^{17}O$ and $^{17}O^{18}O$ is presented in Fig. 3. Note that the abundance of $^{17}O^{18}O$ in the present ^{17}O spectra is almost the same as in our ^{18}O spectra [2], where we were able to detect 45 additional lines which are hidden by much stronger $^{16}O^{17}O$ lines in the present ^{17}O recordings (see Fig. 3).

We provide as Supplementary Material the global RT line list of $^{17}O_2$, $^{16}O^{17}O$ and $^{17}O^{18}O$ including line positions and the experimental values of the intensities corresponding to the relative abundances listed in Table 1.

4. Theoretical background

As mentioned above the ^{17}O oxygen isotopologues have a non-zero nuclear spin I=5/2 and the coupling of the nuclear spin to electron spin in the $X^3\Sigma_g^-$ state [2] and to the electronic angular momentum in the $a^1\Delta_g$ state [7] gives rise to a magnetic hyperfine structure.

The Hamiltonian for the three considered ^{17}O isotopologues can be expressed as [4,5]

$$H = H_{RFS} + H_{HFS} \tag{1}$$

where H_{RFS} corresponds to the rotational and fine structure terms and H_{HFS} to the hf term. The expression of H_{RFS} in the $X^3\Sigma_g^-$ ground state is the following:

$$H_{RFS} = B\mathbf{N}^2 - D\mathbf{N}^4 + H\mathbf{N}^6 + \left[\lambda + \lambda_D\mathbf{N}^2 + \lambda_H\mathbf{N}^4\right]\frac{2}{3}\left(3S_z^2 - \mathbf{S}^2\right) + \left[\gamma + \gamma_D\mathbf{N}^2 + \gamma_H\mathbf{N}^4\right]\mathbf{N}\cdot\mathbf{S} \tag{2}$$

where B, λ and γ are rotational, spin–spin and spin–rotation interaction constants, respectively, while the other constants are their first and second order centrifugal distortion terms. Since no Λ-type doubling was observed, the rotational energies in the $a^1\Delta_g$ state have a simple expression

$$F_v(J) = T_v + B_v J(J+1) - D_v[J(J+1)]^2 + H_v[J(J+1)]^3 \tag{3}$$

The hyperfine structure Hamiltonian can be written as

$$H_{HFS} = aI_zL_z + b_F\mathbf{I}\cdot\mathbf{S} + c(I_zS_z - \tfrac{1}{3}\mathbf{I}\cdot\mathbf{S}) + \frac{e\mathbf{Q}q(3I_z^2 - \mathbf{I}^2)}{4I(2I-1)} \tag{4}$$

where the first term describes the interaction of the electronic orbital moment with the nuclear spin, the second and third terms give information on the electron spin distribution within the molecule. In particular, the Fermi contact parameter b_F is the measure of the spin density at the nucleus, whilst c is associated with angular spin distributions $\langle(3\cos^2\theta-1)/r^3\rangle_s$, where the averaging is over space coordinates for the states in question, r being the distance between unpaired electron and the ^{17}O nucleus and θ being the angle between the **r** vector and the internuclear axis. The fourth term corresponds to the electric quadrupole interaction due to asymmetric charge distribution around the nucleus [17]. In the $X^3\Sigma_g^-$ ground state, Λ=0 and therefore the first term vanishes.

In the case of the $^{16}O^{17}O$ and $^{17}O^{18}O$ species, I=5/2 and then F= J+5/2, J+3/2,… $|J-5/2|$. The rotational levels are then split into six components for $J>2$.

In the case of the $^{17}O_2$ isotopologue, the vectorial addition of the two nuclear spins (I_1=I_2=5/2) leads to six values of the total nuclear spin I_{tot}=I_1+I_2,… $|I_1-I_2|$=5, 4, 3, 2, 1, 0. In the $X^3\Sigma_g^-$ ground state because of the nuclear spin function symmetry, the even and odd values of N'' can only be associated with odd and even values of I''_{tot}, respectively [5]. Fig. 4 shows the hyperfine splitting in the lower (N''=J''=1) and upper (N'=J'=2) states of the R1R1 transition. The N''=1 level can be associated only with I''=0, 2, 4 and then F''=1, 2, 3, 4 and 5, while in the N'=2, upper state, the six I' values are possible and then F' varies from zero to seven.

The $a^1\Delta_g$ upper state is a singlet state (S=0), so that only the first and fourth interaction terms remain in Eq. (4).

The hyperfine component separations decrease with increasing J values, i.e. in the different branches, the

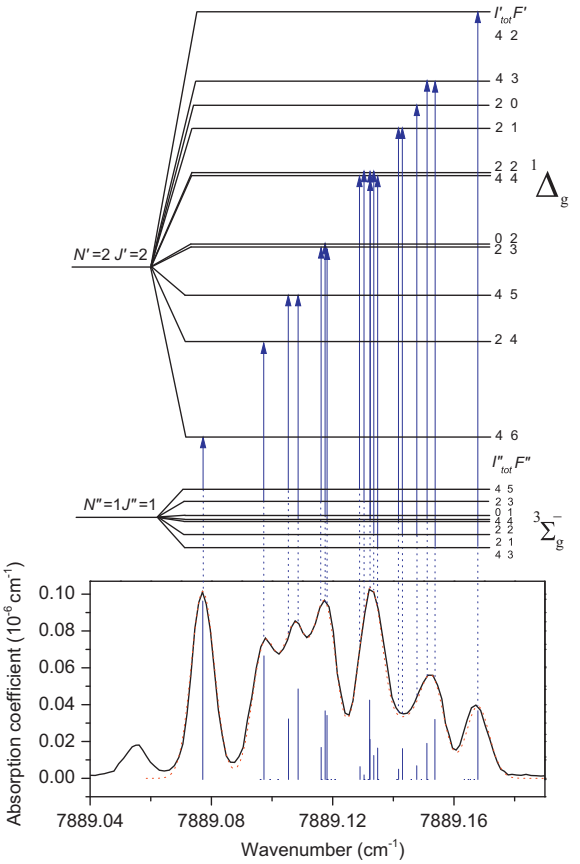

Fig. 4. Energy diagram and spectrum at 80 K of the hyperfine structure of the R1R1 transition of $^{17}O_2$. The black solid line corresponds to the experimental spectrum while the red dash line is a simulation based on the calculated hf structure (stick spectrum). Note that the energy scale of the hyperfine levels corresponds to the wavenumber scale of the spectrum. The line at the left hand side of the spectrum is a $^{16}O^{18}O$ transition. For clarity, the upper state hf levels with odd I_{tot}, from which no transitions are allowed to the lower N''=J''=1, are ignored in this figure.

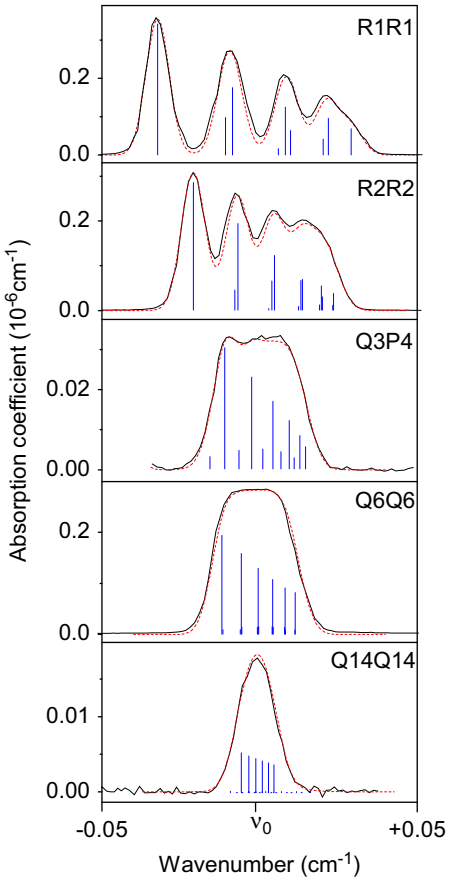

Fig. 5. Hyperfine structure of different $^{16}O^{17}O$ transitions (T=80 K, P=1.5 Torr). The wavenumber values corresponding to the center of the spectral range of each panel (ν_0) are the following: R1R1—7888.5906 cm^{-1}, R2R2—7891.2606 cm^{-1}, Q3P4—7884.8424 cm^{-1}, Q6Q6—7882.3106 cm^{-1}, Q14Q14—7879.0650 cm^{-1}. The black solid line corresponds to the experimental spectrum while the red dash line is a simulation based on the calculated stick spectrum (in blue). (For interpretation of the references to color in this figure legend, the reader is referred to the web version of this article.)

transitions from low rotational levels are expected to show the most resolved hf structure [3]. As an example, Fig. 5 illustrates the evolution of the hf structure with an increasing rotational excitation for $^{16}O^{17}O$. It is worth mentioning that Λ-doubling could not be resolved in the present experiment.

The selection rules for $^{16}O^{17}O$, $^{17}O^{18}O$ and $^{17}O_2$ magnetic dipole transitions are ΔJ=0, $\pm$1 and ΔF=0, $\pm$1. The allowed transitions of the R1R1 line together with the corresponding experimental spectrum of $^{17}O_2$ are included in Fig. 4. For clarity of the figure, only the strongest of the 39 hyperfine components are represented. A similar figure was included in Ref. [3] for the R1R1 transition of $^{16}O^{17}O$. For the high J values, only the hyperfine transitions with ΔJ=ΔF are significant and the intensities are proportional to (2F+1) [18]. The hf coupling terms being identical for $^{16}O^{17}O$ and $^{17}O^{18}O$, these isotopologues show very similar hf structures [3].

5. Spectroscopic parameter derivation

The SPFIT software [19] was used to fit the measured line positions. In the first iteration, we focused on the derivation of the hyperfine coupling constants and the LNT data set was combined with the MW measurements from Cazzoli et al. [4,5]. As mentioned above, only the lowest rotational transitions of the LNT spectra were used as higher rotational transitions are mostly unresolved. In case of blended lines, we assigned all the underlying components of sufficient intensity (more than 1%) to one line center and weighted them according to their calculated relative intensities. The rotational part of the Hamiltonian in the ground $X^3\Sigma_g^-$ and upper $a^1\Delta_g$ electronic states were fit to Eqs. (2) and (3), respectively. Since only few low rotational transitions were considered, the centrifugal distortion constants could not be determined and were held fixed to the values determined in our previous work [2] for $^{16}O^{17}O$ and $^{17}O^{18}O$ and to the values from Ref. [20] for $^{17}O_2$.

In a second step, we completed the input data with the RT data set. Using the SPFIT option allowing to exclude these lines from the fit of the hf parameters, the global fit including all the transitions of the (0–0) band and (1–1) hot band, was performed and provided both the hf coupling constants and the rotational constants (including the centrifugal distortion constants).

As mentioned above, the RT line positions were taken as an average value over the line profile. In consequence, the uncertainties assigned to the $^{17}O_2$, $^{16}O^{17}O$ and $^{17}O^{18}O$ transitions were increased up to 10×10^{-3} cm^{-1} for some low J values.

The $^{17}O_2$ lines of the $a^1\Delta_g$–$X^3\Sigma_g^-$ (0–0) band measured in this work were fitted together with MW lines from Cazzoli et al. [5]. The lines of the $a^1\Delta_g$–$X^3\Sigma_g^-$ (1–1) band together with Raman measurements of the fundamental band in the $X^3\Sigma_g^-$ state [6] were fitted separately, because even the fine structure was not resolved by Edwards et al. [6]. In this fit we fixed the constants of the v=0 levels of the $X^3\Sigma_g^-$ and $a^1\Delta_g$ states to their fitted values and excluded the hf parameters. Raman line centers were included in the fit with large uncertainties (0.015 cm^{-1}).

Unlike $^{17}O_2$, to the best of our knowledge no Raman data are available in the literature for the $^{16}O^{17}O$ species. Thus we were not able to determine the absolute energy term values of the $X^3\Sigma_g^-$ (v=1) and $a^1\Delta_g$ (v=1) states. The $^{16}O^{17}O$ lines of the $a^1\Delta_g$–$X^3\Sigma_g^-$ (0–0) and (1–1) bands were fitted separately and the energy term value of the $X^3\Sigma_g^-$ (v=1) level was fixed to the value (1533.55 cm^{-1}) extrapolated from that of $^{16}O_2$ isotopologue using the usual dependence of the vibrational frequency versus the reduced mass.

Due to the low abundance of $^{17}O^{18}O$ in the sample (about 1%), the $^{17}O^{18}O$ transitions are very weak, which increased the experimental uncertainty on the line position values. The lines from the present ^{17}O spectra were used as the primary source of the input data of the fit and then completed by 45 $^{17}O^{18}O$ lines, which were previously measured in the ^{18}O enriched spectrum [2] and are blended or hidden in the ^{17}O spectra.

The results of the fit are given in Table 2. The *rms* values corresponding to our data (2.07×10^{-3},

Table 2
Spectroscopic parameters (cm^{-1}) of the $v=0$ and $v=1$ levels of the $X^3\Sigma_g^-$ and $a^1\Delta_g$ states of $^{16}O^{17}O$, $^{17}O^{18}O$ and $^{17}O_2$.

Parameters	$^{16}O^{17}O$		$^{17}O^{18}O$		$^{17}O_2$			
	$X^3\Sigma_g^-$							
	$v=0$	$v=1$	$v=0$		$v=0$		$v=1$	
E		[a]					1510.3649(44)	
B	1.3953322(27)	1.380238(40)	1.3154953(23)		1.3529818(11)		1.338575(56)	
D	$-4.5615(21)\times10^{-6}$	$-4.533(78)\times10^{-6}$	$-4.0535(39)\times10^{-6}$		$-4.2893(19)\times10^{-6}$		$-4.26(14)\times10^{-6}$	
λ	1.98471099(30)	1.98849(82)	1.98463272(69)		1.98466915(12)		1.9860(12)	
λ_D	$1.8885(37)\times10^{-6}$		$1.7835(95)\times10^{-6}$		$1.82771(88)\times10^{-6}$			
γ	$-8.176545(78)\times10^{-3}$	$-8.207(63)\times10^{-3}$	$-7.70714(12)\times10^{-3}$		$-7.927372(21)\times10^{-3}$		$-8.23(11)\times10^{-3}$	
γ_D	$-6.99(58)\times10^{-9}$		$-7.3(12)\times10^{-9}$		$-7.199(88)\times10^{-9}$			
b_F	$-1.82607(31)\times10^{-3}$		$-1.82610(70)\times10^{-3}$		$-1.826529(78)\times10^{-3}$			
c	$4.67255(79)\times10^{-3}$		$4.6729(20)\times10^{-3}$		$4.67116(21)\times10^{-3}$			
eQq	$-2.713(80)\times10^{-4}$		$-2.74(16)\times10^{-4}$		$-2.769(13)\times10^{-4}$			
	$a^1\Lambda_g$							
	$v=0$	$v=1$	$v=0$		$v=0$		$v=1$	
T	7884.45452(11)	7812.63054(91)[b]	7885.78877(16)		7885.15500(12)		9324.8176(48)	
B	1.3760896(29)	1.359745(42)	1.2973722(28)		1.3343330(13)		1.318697(58)	
D	$-4.8107(24)\times10^{-6}$	$-4.783(81)\times10^{-6}$	$-4.2743(47)\times10^{-6}$		$-4.5235(20)\times10^{-6}$		$-4.43(13)\times10^{-6}$	
a	$-7.250(65)\times10^{-3}$		$-7.055(87)\times10^{-3}$		$-7.069(42)\times10^{-3}$			
Number of lines[c]	Total:345		Total: 180		Total: 793			
	MW: 59	This work[d]: 218	MW: 30	This work[d]: 105+45[e]	MW: 516	This work[d]: 215	Raman: 23	This work: 39
rms[f]	4.48×10^{-2} MHz	2.08×10^{-3} cm^{-1}	5.58×10^{-2} MHz	2.39×10^{-3} cm^{-1}	7.11×10^{-2} MHz	2.07×10^{-3} cm^{-1}	9.75×10^{-3} cm^{-1}	3.03×10^{-3} cm^{-1}

[a] The energy term value of $X^3\Sigma_g^-$ ($v=1$) was estimated to be $E=1533.55$ cm^{-1} using the corresponding value of $^{16}O_2$ and the mass dependence of the vibrational frequency (see Text).
[b] Difference between the energy term values of the $v=1$ levels in the ground $X^3\Sigma_g^-$ and excited $a^1\Delta_g$ states (see text).
[c] Microwave (MW) and Raman data were taken from Refs. [4,5] and Ref. [6], respectively.
[d] The hyperfine components were not counted; one hf manifold was considered as one line.
[e] 45 additional lines measured in Ref. [2] were included in the fit.
[f] $\mathrm{rms}=\sqrt{\left(\sum_i(\sigma_{obs}-\sigma_{calc})_i^2\right)/(N-p)}$, where the summation applies to the N experimental data of a given source and p is the number of fitted parameters.

2.08×10^{-3} and 2.39×10^{-3} cm^{-1} for $^{17}O_2$, $^{16}O^{17}O$ and $^{17}O^{18}O$, respectively) are satisfactory, considering the large uncertainty on some line centers.

Note that we have tried to fit the quadrupole coupling constant of the $a^1\Delta_g$ (last term in Eq. (4)) but it could not be well determined. The corresponding constant in the ground state of $^{16}O^{17}O$ and $^{17}O^{18}O$ is about -8 MHz and according to the calculations of Minaev and Minaeva [21] it should be similar in the excited state and then too small to be determined from our near infrared spectra.

We have superimposed to the spectra of Figs. 4 and 5 a simulation of the hf structure calculated with the fitted parameters values. The simulated spectra were obtained by affecting a Doppler line profile (at 80 K) to the stick spectrum provided by the SPFIT program. It leads to a very good agreement between the measured and calculated spectra.

The results of the fit of the spectroscopic parameters of each of the $^{17}O_2$, $^{16}O^{17}O$ and $^{17}O^{18}O$ isotopologues are provided as Supplementary Material. The supplementary files include the complete set of wavenumber values measured in this work together with microwave and Raman measurements when available and the corresponding (obs.-calc.) values.

6. Discussion

Our fitted values of the hf coupling constants for the $a^1\Delta_g$ state are reproduced in Table 3 in MHz units and compared with the value determined by Arrington et al. from a fit of EPR spectra [7]. Since in theory there is no isotopic dependence for this parameter, these authors performed a global fit for the two species and determined the coupling constant to be -424 ± 1 MHz, which is almost exactly a factor of 2 greater than our values (-217.3 ± 1.9 and -211.5 ± 2.6 MHz, for $^{16}O^{17}O$ and $^{17}O^{18}O$, respectively). This factor of 2 difference is merely due to the different definition of the coupling constant in the work of Arrington et al. [7], where the value of Λ ($\Lambda=2$ in this case) is absorbed into the constant.

The ground-state hyperfine structure of $^{16}O^{17}O$, $^{17}O^{18}O$ and $^{17}O_2$ has been previously investigated in the microwave and millimeter ranges [4,5,22–24]. The comparison with the hf coupling constants of $^{16}O^{17}O$ and $^{17}O^{18}O$ in the ground state obtained by Cazzoli et al. [4] is not straightforward as they used a different parameters for the Hamiltonian corresponding to the magnetic part of the hyperfine splitting

$$H_{HFS}=b\mathbf{I}\cdot\mathbf{S}+c\,I_zS_z \tag{5}$$

The minor difference with our Eq. (4) is that the isotropic and anisotropic contributions are not completely separated and therefore Eq. (5) yields less valuable physical information. Nevertheless, to make direct comparison we have fitted the CRDS and MW data using the magnetic contribution as given in Eq. (5). The results of this fit are given in Table 4 together with the values from Cazzoli et al. [4]. There appears to be a good agreement in all the constants except c where a slight disagreement is apparent. The reason for this discrepancy is unclear, but one can note that our value of c for $^{16}O^{17}O$ is close to the one reported by Gerber from EPR spectroscopy measurements [24]. We have also fitted only the MW lines from Ref. [4] and the discrepancy with the value of c reported in [4] remained, while the residuals in our fit were smaller.

In the work of Cazzoli et al. [5] devoted to $^{17}O_2$ the corresponding part of the Hamiltonian is given as:

$$H_{HFS}=\alpha\mathbf{I}\cdot\mathbf{S}+\beta(3I_zS_z-\mathbf{I}\cdot\mathbf{S}) \tag{6}$$

where the isotropic and anisotropic parts are separated. This expression is similar to our Eq. (4) where our b_F and c constants correspond to α and 3β, respectively. The comparison of our hyperfine parameters obtained using Eq. (4) with those given in Ref. [5] is also given in Table 4 and shows a very good agreement.

Table 3
The hf coupling parameter (MHz) of the $a^1\Delta_g$ state of $^{16}O^{17}O$, $^{17}O^{18}O$ and $^{17}O_2$.

	$^{16}O^{17}O$	$^{17}O^{18}O$	$^{17}O_2$
This work[a]	−217.35(195)	−211.50(261)	−211.93(126)
[7][a]	−424(1)[a]	−424(1)[a]	

[a] The difference by a factor of 2 compared to our values is due to a different definition (see text for details).

Table 4
Comparison of the hf coupling parameters of the $X^3\Sigma_g^-$ state of $^{16}O^{17}O$, $^{17}O^{18}O$ and $^{17}O_2$.

Parameter (MHz)	$^{16}O^{17}O$	$^{17}O^{18}O$	$^{17}O_2$
b [a] (This work)	−101.4356(34)	−101.4416(62)	−54.7580(24)
b [4,5]	−101.441(5)	−101.46(1)	−54.758(3)
c (This work)	140.095(23)	140.090(59)	140.0378(62)
c [4,5]	139.73(3)	139.68(6)	140.037(9)[b]
c [24]	140.123(36)	…	…
eQq (This work)	−8.13(24)	−8.23(47)	−8.302(39)
eQq [4,5]	−8.3(3)	−7.8(5)	−8.29(3)

[a] For comparison purpose, the hf parameters of $^{16}O^{17}O$ and $^{17}O^{18}O$ were fitted using the same hf Hamiltonian that was used in Ref. [4] (Eq. (5)). In consequence, the obtained b values differ from those included in Table 2. The value given for $^{17}O_2$ is the b_F value listed in Table 2 (Eq. (4)) (see text for details).

[b] The value given here is three times the value of Ref [5] due to a different definition.

7. Conclusion

The spectroscopic knowledge of the $a^1\Delta_g$–$X^3\Sigma_g^-$ band of the three ^{17}O-containing oxygen isotopologues – $^{16}O^{17}O$, $^{17}O^{18}O$ and $^{17}O_2$ – has been considerably extended from CRDS spectra at room temperature and at 80 K. The hyperfine structure of the low rotational transitions of the $a^1\Delta_g$–$X^3\Sigma_g^-$ band has been observed for the first time. The spectroscopic fit of the different $a^1\Delta_g$–$X^3\Sigma_g^-$ transitions measured in this work and available microwave and Raman data provide the best to date set of spectroscopic data for the $a^1\Delta_g$ state of $^{16}O^{17}O$, $^{17}O^{18}O$ and $^{17}O_2$. For the $^{17}O_2$ isotopologue, these $a^1\Delta_g$ parameters including hf coupling parameter were determined for the first time. The resulted parameters were used for the simulation of the hf structure, which shows a very good reproduction of the measured hf structure. The new observation of electric

quadrupole transitions in the $a^1\Delta_g - X^3\Sigma_g^-$ system of $^{16}O^{17}O$ and $^{17}O_2$ species is reported together with the first determined spectroscopic constants for $a^1\Delta_g$ $v=1$ state of these species. The results of this work can be used for accurate prediction of spectral line parameters of ^{17}O-containing species. For instance, the $^{16}O^{17}O$ transitions can be potentially found in the atmospheric spectra as their strength is similar to the electric quadrupole transitions of $^{16}O_2$ that were already identified in the solar atmospheric spectrum [1].

Acknowledgments

Part of this work was performed at Grenoble University under the ANR project "IDEO" (NT09_436466). A portion of this research was performed at Jet Propulsion Laboratory, California Institute of Technology and Harvard-Smithsonian Center for Astrophysics, under contract with the National Aeronautics and Space Administration.

Appendix A. Supporting material

Supplementary data associated with this article can be found in the online version at doi:10.1016/j.jqsrt.2011.01.014.

References

[1] Gordon IE, Kassi S, Campargue A, Toon GC. First identification of the $a^1\Delta_g - X^3\Sigma_g^-$ electric quadrupole transitions of oxygen in the solar and laboratory spectra. J Quant Spectrosc Radiat Transfer 2010;111:1174–83.

[2] Leshchishina O, Kassi S, Gordon IE, Rothman LS, Wang L, Campargue A. High sensitivity CRDS of the $a^1\Delta_g - X^3\Sigma_g^-$ band of oxygen near 1.27 μm: extended observations, quadrupole transitions, hot bands and minor isotopologues. J Quant Spectrosc Radiat Transfer 2010;111:2236–45.

[3] Kassi S, Leshchishina O, Gordon IE, Yu S, Campargue A. Hyperfine structure of the $a^1\Delta_g - X^3\Sigma_g^-$ transitions of $^{16}O^{17}O$, $^{17}O^{18}O$ and $^{17}O_2$ by CRDS at 80 K. Chem Phys Lett. 2011;502:37–41.

[4] Cazzoli G, Degli Esposti C, Favero PG, Severi G. Microwave spectra of $^{16}O^{17}O$ and $^{18}O^{17}O$. Nuovo Cimento B Serie 1981;62:243–54.

[5] Cazzoli G, Degli Esposti C, Landsberg BM. Millimetre wave spectrum of $^{17}O_2$. Magnetic hyperfine structure and quadrupole coupling constants. Nuovo Cimento D Serie 1984;3:341–60.

[6] Edwards HGM, Long DA, Najm KAB, Thomsen M. The vibration-rotation Raman spectra of $^{18}O_2$,$^{17}O^{18}O$,$^{17}O_2$ and $^{16}O_2$. J Raman Spectrosc 1981;10:60–3.

[7] Arrington Jr. CA, Falick AM, Myers RJ. Electron paramagnetic resonance spectrum of O_2 ($a^1\Delta_g$)—its ^{17}O hyperfine coupling and electronic and rotational g values. J Chem Phys 1971;55:909–14.

[8] Macko P, Romanini D, Mikhailenko SN, Naumenko OV, Kassi S, Jenouvrier A, et al. High sensitivity CW-cavity ring down spectroscopy of water in the region of the 1.5 μm atmospheric window. J Mol Spectrosc 2004;227:90–108.

[9] Morville J, Romanini D, Kachanov AA, Chenevier M. Two schemes for trace detection using cavity ringdown spectroscopy. Appl Phys 2004;D78:465–76.

[10] Perevalov BV, Kassi S, Romanini D, Perevalov VI, Tashkun SA, Campargue A. CW-cavity ringdown spectroscopy of carbon dioxide isotopologues near 1.5 μm. J Mol Spectrosc 2006;238:241–55.

[11] Kassi S, Gao B, Romanini D, Campargue A. The near-infrared (1.30–1.70 μm) absorption spectrum of methane down to 77 K. Phys Chem Chem Phys 2008;10:4410–9.

[12] Kassi S, Romanini D, Campargue A. Mode by mode CW-CRDS at 80 K: application to the 1.58 μm transparency window of CH_4. Chem Phys Lett 2009;477:17–21.

[13] Wang L, Kassi S, Liu A, Hu S, Campargue A. The 1.58 μm transparency window of methane (6165–6750 cm^{-1}): empirical line list and temperature dependence between 80 K and 296 K. J Quant Spectrosc Radiat Transfer, in press. doi:10.1016/j.jqsrt.2010.11.015.

[14] Wang L, Kassi S, Liu A, Hu S, Campargue A. High sensitivity absorption spectroscopy of methane at 80 K in the 1.58 μm transparency window: temperature dependence and importance of the CH_3D contribution. J Mol Spectrosc 2010;261:41–52.

[15] Rothman LS, Gordon IE, Barbe A, Benner DC, Bernath PF, Birk M, et al. The HITRAN 2008 molecular spectroscopic database. J Quant Spectrosc Radiat Transfer 2009;110:533–72 Updated oxygen: http://www.cfa.harvard.edu/HITRAN/Updated/07_hit09.par.

[16] Babcock HD, Herzberg L. Fine structure of the red system of atmospheric oxygen bands. Astrophys J 1948;108:167–90.

[17] Frosh RA, Foley HM. Magnetic hyperfine structure in diatomic molecules. Phys Rev 1952;88:1337–49.

[18] Townes CH, Schawlow AK. Microwave spectroscopy. New York: Dover; 1975.

[19] Pickett HM. The fitting and prediction of vibration-rotation spectra with spin interactions. J Mol Spectrosc 1991;148:371–7.

[20] 〈http://physics.nist.gov/PhysRefData/MolSpec/Diatomic/Html/Tables/O2.html〉.

[21] Minaev BF, Minaeva VA. MCSCF response calculations of the excited states properties of the O_2 molecule and a part of its spectrum. Phys Chem Chem Phys 2001;3:720–9.

[22] Long DA, Havey DK, Okumura M, Miller CE, Hodges JT. Cavity ringdown spectroscopy measurements of sub-Doppler hyperfine structure. Phys Rev 2010;81:064502–5.

[23] Miller SL, Townes CH. The microwave absorption spectrum of ^{16}O) and $O^{16}O^{17}$. Phys Rev 1953;90:537–42.

[24] Gerber P. Hyperfeinstruktur des Elektronenspinresonanzspektrums von molekularem Sauerstoff in der Gasphase. Helv Phys Acta 1972;45:655.